Hindawi Publishing Corporation
Journal of Applied Mathematics
Volume 2013, Article ID 679071, 10 pages
http://dx.doi.org/10.1155/2013/679071

Research Article

Modeling and Parameter Analysis of the OC3-Hywind Floating Wind Turbine with a Tuned Mass Damper in Nacelle

Yulin Si,[1] Hamid Reza Karimi,[1] and Huijun Gao[2]

[1] *Department of Engineering, Faculty of Engineering and Science, University of Agder, N4898 Grimstad, Norway*
[2] *Research Institute of Intelligent Control and Systems, Harbin Institute of Technology, Harbin 150001, China*

Correspondence should be addressed to Yulin Si; yulin.si@uia.no

Received 12 August 2013; Accepted 10 October 2013

Academic Editor: Dewei Li

Floating wind turbine will suffer from more fatigue and ultimate loads compared with fixed-bottom installation due to its floating foundation, while structural control offers a possible solution for direct load reduction. This paper deals with the modelling and parameter tuning of a spar-type floating wind turbine with a tuned mass damper (TMD) installed in nacelle. First of all, a mathematical model for the platform surge-heave-pitch motion and TMD-nacelle interaction is established based on D'Alembert's principle. Both intrinsic dynamics and external hydro and mooring effects are captured in the model, while tower flexibility is also featured. Then, different parameter tuning methods are adopted to determine the TMD parameters for effective load reduction. Finally, fully coupled nonlinear wind turbine simulations with different designs are conducted in different wind and wave conditions. The results demonstrate that the design of TMD with small spring and damping coefficients will achieve much load reduction in the above rated condition. However, it will deteriorate system performance when the turbine is working in the below rated or parked situations. In contrast, the design with large spring and damping constants will produce moderate load reduction in all working conditions.

1. Introduction

With less space constraints and more consistent wind, offshore deep sea wind energy has attracted great worldwide attention in recent years. Wind turbines in deep water are usually installed at places where sea depth is between 60 m and 900 m; thus, floating foundations are generally considered to be an economical and feasible way of deployment [1]. Based on decades of experience from offshore oil and gas industry, several different traditional floating platforms have been proposed to support large wind turbines in deep sea regions, including spar-buoy, tension leg, barge, and semisubmersible [2]. One of the most promising concepts is the spar-type supporting structure, based on which one Norwegian company Statoil has developed the world first experimental large floating offshore wind turbine in 2009.

Different from fixed-bottom wind turbines, the very first challenge for floating windmills is the wave and wind induced platform tilt motion, which will heavily increase the loads on turbine structure due to high inertial and gravitational forces [3]. According to [4], when comparing a barge-type floating wind turbine with an onshore design, the sea-to-land ratio of fatigue loads with respect to tower base bending moments has reached 7. The ratio is still over 1.5 for the OC3-Hywind spar, which may require extra reinforcement or advanced control technique to improve wind turbine reliability. Besides, soft foundation properties of floating wind turbines will lead to low natural frequency platform motion, so that commonly used blade pitch control strategy for fixed-bottom wind turbines may cause negative damping of tower bending and even large platform resonant motion [5]. These problems have drawn a lot of attention from researchers on improving the system design and control strategy of floating wind turbines for load reduction.

One approach for vibration inhibition is to utilize structural vibration control devices. This method has been successfully applied in civil engineering structures [6], such as buildings and bridges, and thus is also expected to be a promising solution for extending the fatigue life of floating wind turbines. In [7], Murtagh et al. investigated the use of

a tuned mass damper (TMD) placed at the tower top for the vibration mitigation due to the along-wind forced vibration response of a simplified wind turbine. Following the same installation idea, Colwell and Basu explored the structural responses of fixed-bottom offshore wind turbines with tuned liquid column dampers (TLCD) to control the vibrations [8]. Moreover, Li et al. performed an experimental study on an offshore wind turbines with a ball vibration absorber fixed on top of the nacelle [9]. However, these discussions are about vibration mitigation of fixed-bottom wind turbines, while their dynamics are quite different from that of floating ones. Besides, these works are not based on the cutting edge high-fidelity codes for wind turbine simulations, which cannot capture the comprehensive coupled nonlinear dynamics of wind turbines.

FAST (fatigue, aerodynamics, structures, and turbulence) is one of the state-of-the-art aero-hydro-servo-elastic wind turbine numerical simulators [10]. Based on FAST, Lackner and Rotea implemented a new simulation tool, called FAST-SC, for passive, semiactive, and active structural control design of wind turbines [11]. Utilizing this code, Lackner and Rotea presented more realistic simulation results with a TMD installed in the nacelle of either a barge-type or a monopile supported wind turbine, and a simple parametric study was also performed to determine the optimal TMD parameters [11]. Further, it was shown that more load reduction could be achieved when introducing active structural control in their following works [12, 13]. In order to perform a more comprehensive parametric study of passive structural control design, the authors in [14, 15] established a 3-DOF dynamic model for different types of floating wind turbines based on first principles. This limited DOF model has greatly facilitated the parameter analysis and active control design, while the coupling between surge and pitch motion, however, was not captured, which can be ignored for the barge design but might be an important mode for other platforms, such as spar [16, 17].

Motivated by the above-mentioned problems and research potentials, this work focuses on modeling and parameter analysis of a passive structural control design for a spar-type floating wind turbine. The remainder of this paper is organized as follows. Section 2 introduces the OC3-Hywind floating wind turbine, and the coupled surge-heave-pitch dynamic model with a TMD installed in nacelle is established. Parameter estimation is also performed for model validation. In Section 3, different parameter tuning methods and performance indices are used for TMD parameter determination. Section 4 presents the nonlinear simulation results under different wind and wave conditions. Advantages and limitations of this design with different TMD parameters are also analyzed. At last, we draw conclusions in Section 5.

2. Dynamic Modelling

In cooperation with Statoil, Jonkman from NREL has specified a detailed OC3-Hywind spar-type floating wind turbine model, which is a combination of the data for the 5MW baseline wind turbine from NREL and the Hywind floating platform from Statoil [16, 18]. Properties of the OC3-Hywind model are shown in Table 1. According to [16], in order to avoid resonant platform pitch motion, the conventional controller in Region 3 is modified into a combination of gain reduced gain-scheduled proportional-integral (GSPI) collective blade pitch control and constant torque control, which is used all through this work as the baseline.

Table 1: Properties of the OC3-Hywind model [16, 18].

Item	Value
Rating	5 MW
Rotor configuration	Upwind, 3 blades
Cut-in, rated, cut-out wind speed	3 m/s, 11.4 m/s, 25 m/s
Total draft below sea water level (SWL)	120 m
Tower base above SWL	10 m
Hub height above SWL	90 m
Nacelle dimension (length, width, height)	14.2 m, 2.3 m, 3.5 m
Platform diameter above taper	6.5 m
Platform diameter below taper	9.4 m
Rotor nacelle assembly (RNA) mass	350,000 kg
Tower mass	249,718 kg
Platform mass	7,466,000 kg
Number of mooring lines	3
Depth to fairleads below SWL	70 m
Baseline control in Region 3	GSPI and constant torque

The passive structural control strategy in this work is to install one TMD in the nacelle, which is assumed to move on an ideal nonfriction linear track along the fore-aft direction. The stiffness and damping parameters of TMD can be tuned, and they are regarded as constant in all simulations. In order to investigate these parameters, optimize system performance, or design an active controller, establishing one dynamic mathematical model is usually helpful. Figure 1 shows a diagram of the OC3-Hywind surge-heave-pitch motion with tower fore-aft bending and the TMD-nacelle interaction. Definition of each term in this figure can be found in Table 2. Before presenting the dynamic model, the following premises and assumptions need to be listed.

(1) OC3-Hywind is treated as a multibody dynamic system, and the motion of reference point P is chosen for output analysis, which is in accordance with the definition in [16]. Rigid bodies in the model include the spar platform, tower, and rotor nacelle assembly (RNA). Dynamics in rotor, generator, and gearbox are not considered in this work.

(2) Based on the same assumption, the tower fore-aft flexibility is represented as that in [13], where the tower, for simplicity, is treated as a linear rigid rotating beam hinged at tower bottom. It is also assumed that the spring and damping coefficients of this hinge are constant.

Table 2: Term descriptions in the model of OC3-Hywind surge-heave-pitch motion.

Terms	Descriptions
sg	DOF of platform surge motion
hv	DOF of platform have motion
p	DOF of platform pitch motion
tmd	DOF of TMD motion
t	DOF of tower fore-aft bending
θ_i	Rotation angle of DOF i
x_i	Displacement of DOF i
M_i^j	Generalized mass for DOF i with regard to DOF j
I_i^j	Generalized inertia tensor for DOF i with regard to DOF j
F_i^j	Generalized force for DOF i due to effect or DOF j
τ_i^j	Generalized torque for DOF i due to effect or DOF j
gr	Gravitational effect
hdr	Hydro effect
ctr	Centripetal effect
moor	Mooring lines effect
spr.damp	Spring and damping effect of TMD
A_i^j	Generalized added mass for DOF i with regard to DOF j
J_u^X	Inertia tensor for u with regard to point X
L_u	Length of part u
m_u	Mass of part u
ptfm	Platform
twr	Tower
rna	Rotor nacelle assembly (RNA)
d	Misalignment between RNA mass center and tower centerline
jot	Joint between platform and tower
D_i^j	Equivalent damping coefficient for DOF i with regard to DOF j
K_i^j	Equivalent spring coefficient for DOF i with regard to DOF j
g	Gravitational acceleration
CB	Center of buoyancy
CG_u	Gravity center of part u

(3) In total, the model has five DOFs, that is, platform surge, heave, pitch, tower fore-aft bending, and TMD motion. The other DOFs, such as rotor yaw motion and generator rotation, are not included.

(4) This model focuses on the system intrinsic coupled dynamics with hydro and mooring loads, while the loads from winds and incident waves have not yet been considered in the modelling process.

Based on the above descriptions, we treat the overall system dynamics as the motion of a rigid body with distributed mass particles in the surge-heave-pitch plane, which can be seen as the sum of a translation and a rotation about the axis passing through P and perpendicular to this plane [19].

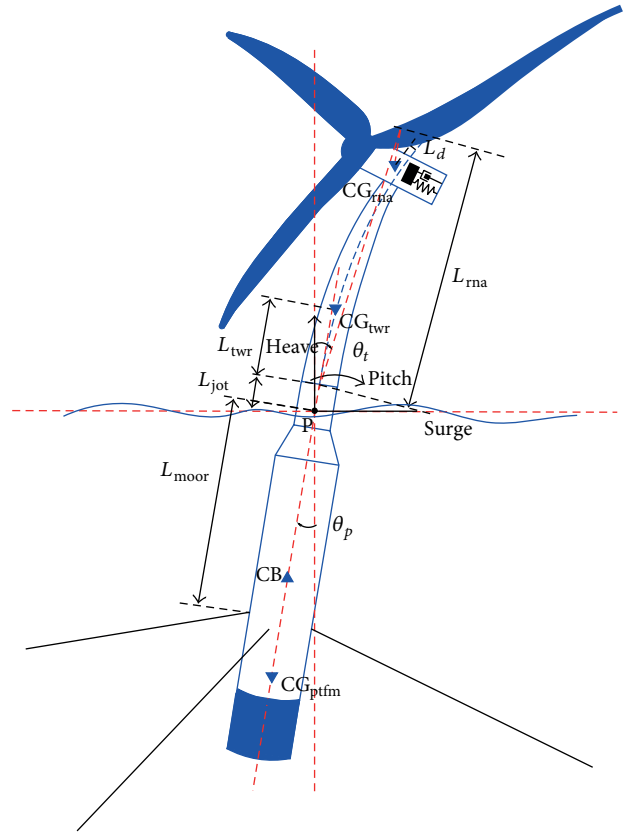

Figure 1: Diagram of the OC3-Hywind surge-pitch-heave motion with tower fore-aft flexibility and passive structural control.

According to D'Alembert's principle of inertial forces, the following static equilibrium equations for system translation and rotation about the reference point P

$$\begin{aligned} \mathbf{F} - \sum m_i \mathbf{a}_i &= 0, \\ \boldsymbol{\tau} - \sum \mathbf{r}_i \times m_i \mathbf{a}_i &= 0, \end{aligned} \tag{1}$$

hold. $\mathbf{F}$ and $\boldsymbol{\tau}$ denote vectors of external forces and moments about P, while $-\sum m_i \mathbf{a}_i$ and $-\sum \mathbf{r}_i \times m_i \mathbf{a}_i$ are vector sums of inertial forces and torques about P. m_i is the mass of particle i, that is, platform, tower, RNA, and TMD, and $\mathbf{r}_i$ represents the position vector from P to particle i. $\mathbf{a}_i$ is the acceleration vector for mass particle i, and it consists of the translational acceleration, normal, and tangential rotational acceleration components.

When considering the tower translation and rotation about tower bottom, the motion of tower fore-aft bending can be described as

$$\sum \left(\mathbf{r}_i \times m_i \mathbf{a}_i\right) + I_t^t \boldsymbol{\alpha}_t = \boldsymbol{\tau}_t^{gr} + \boldsymbol{\tau}_t^p, \tag{2}$$

which is also based on D'Alembert's principle. m_i denotes the mass of tower, RNA, and TMD. I_t^t is the equivalent moment of inertia for tower and RNA about tower bottom, and $\boldsymbol{\alpha}_t$ denotes the angular acceleration vector of tower pitch motion. $\boldsymbol{\tau}_t^p$ is the torque vector due to the spring-damping

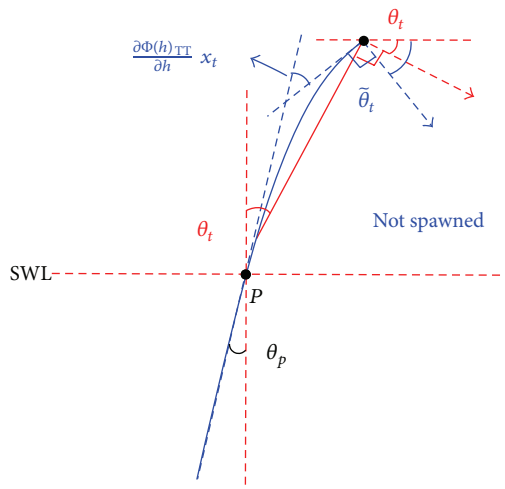

Figure 2: Diagram for calibration of nacelle rotation angle.

effect between tower and platform. To be consistent with the output of FAST simulator, the tower top displacement is also calculated, which is given by

$$x_t = \sin\left(\theta_t - \theta_p\right) l_{\mathrm{twr}}, \tag{3}$$

where l_{twr} is the length of flexible tower. However, in the system validation process, one problem is found which is that there will exist huge misalignment between the responses of FAST-SC and established model when the spring and damping coefficients of TMD are in small scale. This is mainly due to the inaccuracy of nacelle rotation angle when flexible tower is modeled as a rigid rotating beam. When TMD has tiny spring and damping constants, its acceleration will be mainly contributed by gravity, so that inaccuracy of θ_t will lead to tremendous difference of TMD dynamics. Therefore, the nacelle rotation angle should be calibrated in order to produce more convincing dynamic responses. In FAST, the tower flexibility is depicted by the predefined mode shapes Φ, where tower top rotation angle is determined by the product of tower top mode shape slope $\partial\Phi(h)_{\mathrm{rna}}/\partial h$ and tower top displacement x_t. Following similar calculation procedure, the diagram for tower top rotation calibration is illustrated in Figure 2, and the calibrated nacelle rotation angle $\widetilde{\theta}_t$ satisfies

$$\widetilde{\theta}_t = \left.\frac{\partial\Phi(h)}{\partial h}\right|_{h=L_{\mathrm{rna}}} x_t + \theta_p. \tag{4}$$

Next, the hydrodynamic loads are characterized. When formulating the motion of object submerged in water, we must also consider the added-mass effect, resulting from its surrounding fluid [20]. It is summarized in [1] that the hydrodynamic loads mainly include contributions from hydrostatics (from water-plane area and buoyancy), radiation (from outgoing waves generated by platform motion), and diffraction (from incident waves). In accordance with this analysis, the hydrodynamic load calculation in this work follows a similar path. Firstly, hydrostatic load in this model consists of buoyancy force and restoring load resulting from the effects of water-plane area and buoyancy, and the restoring force and moment are set to be constantly proportional to platform displacement and tilt angle which have been specified in [16]. Secondly, the radiation loads can be represented by nonlinear vicious drag, hydrodynamic radiation damping, and the above mentioned added-mass effects. Thirdly, incident wave loads are not considered here since wind turbine is supposed to be located in still water in design process.

Regarding the mooring system, FAST simulator uses a quasistatic model to calculate the load of an individual mooring line, which exhibits nonlinear behaviors due to both mooring dynamics and the asymmetry of the three-point mooring system. In the simulations of this work, the platform displacement and tilt angle are usually not in big scale where the mooring system load-displacement relationship does not show strong nonlinearities in surge and pitch modes, so we still choose the simple linear model to represent this effect.

In sum, except for added mass, the hydrodynamic loads and mooring effect are modeled as

$$\begin{aligned}
F_{\mathrm{sg}}^{\mathrm{hdr\cdot moor}} &= -D_{\mathrm{sg}}^{\mathrm{sg}}\dot{x}_{\mathrm{sg}} - \widehat{D}_{\mathrm{sg}}^{\mathrm{sg}}\dot{x}_{\mathrm{sg}}^2 - K_{\mathrm{sg}}^{\mathrm{sg}}x_{\mathrm{sg}} - D_{\mathrm{sg}}^{p}\dot{\theta}_p - K_{\mathrm{sg}}^{p}\theta_p,\\
F_{\mathrm{hv}}^{\mathrm{hdr\cdot moor}} &= -D_{\mathrm{hv}}^{\mathrm{hv}}\dot{x}_{\mathrm{hv}} - K_{\mathrm{hv}}^{\mathrm{hv}}x_{\mathrm{hv}} - F_{\mathrm{moor}}^{0} + F_{\mathrm{buoy}}^{0}\\
&\quad - K_{\mathrm{hv}}^{p\cdot\mathrm{sg}}\left(x_{\mathrm{sg}} - L_{\mathrm{moor}}\sin\theta_p\right)^2,\\
\tau_p^{\mathrm{hdr\cdot moor}} &= -D_p^p\dot{\theta}_p - K_p^p\theta_p - D_p^{\mathrm{sg}}\dot{x}_{\mathrm{sg}} - \widehat{D}_p^{\mathrm{sg}}\dot{x}_{\mathrm{sg}}^2 - K_p^{\mathrm{sg}}x_{\mathrm{sg}}.
\end{aligned} \tag{5}$$

D_i^j, $\widehat{D}_i^j$, and K_i^j denote equivalent damping and spring coefficients for DOF i with regard to DOF j for the calculation of hydro and mooring effects. F_{moor}^0 and F_{buoy}^0 represent initial mooring line and buoyancy forces when there isno platform displacement or rotation. It should be noted that the mooring load for platform heave motion shows strong nonlinear relationship with the surge and pitch modes; thus, it is not simplified.

Based on the above analysis and equations, the nonlinear dynamic model of OC3-Hywind surge-heave-pitch motion can be established in the following implicit form:

$$\begin{aligned}
&\begin{bmatrix}
M_{\mathrm{sg}}^{\mathrm{sg}} & 0 & I_{\mathrm{sg}}^{p} & M_{\mathrm{sg}}^{\mathrm{tmd}} & I_{\mathrm{sg}}^{t}\\
0 & M_{\mathrm{hv}}^{\mathrm{hv}} & I_{\mathrm{hv}}^{p} & M_{\mathrm{hv}}^{\mathrm{tmd}} & I_{\mathrm{hv}}^{t}\\
M_{p}^{\mathrm{sg}} & M_{p}^{\mathrm{hv}} & I_{p}^{p} & M_{p}^{\mathrm{tmd}} & 0\\
M_{\mathrm{tmd}}^{\mathrm{sg}} & M_{\mathrm{tmd}}^{\mathrm{hv}} & I_{\mathrm{tmd}}^{p} & M_{\mathrm{tmd}}^{\mathrm{tmd}} & I_{\mathrm{tmd}}^{t}\\
M_{t}^{\mathrm{sg}} & M_{t}^{\mathrm{hv}} & 0 & M_{t}^{\mathrm{tmd}} & I_{t}^{t}
\end{bmatrix}
\begin{bmatrix}
\ddot{x}_{\mathrm{sg}}\\ \ddot{x}_{\mathrm{hv}}\\ \ddot{\theta}_p\\ \ddot{x}_{\mathrm{tmd}}\\ \ddot{\theta}_t
\end{bmatrix}\\
&\quad = \begin{bmatrix}
F_{\mathrm{sg}}^{\mathrm{hdr\cdot moor}} + F_{\mathrm{sg}}^{\mathrm{ctr}}\\
F_{\mathrm{hv}}^{\mathrm{gr}} + F_{\mathrm{hv}}^{\mathrm{hdr\cdot moor}} + F_{\mathrm{hv}}^{\mathrm{ctr}}\\
\tau_p^{\mathrm{gr}} + \tau_p^{\mathrm{hdr\cdot moor}} + \tau_p^{\mathrm{ctr}}\\
F_{\mathrm{tmd}}^{\mathrm{gr}} + F_{\mathrm{tmd}}^{\mathrm{spr\cdot damp}}\\
\tau_t^{\mathrm{gr}} + \tau_t^{p} + \tau_t^{\mathrm{ctr}}
\end{bmatrix}.
\end{aligned} \tag{6}$$

In this model, sg, hv, p, tmd, and t represent, respectively, the enabled 5 DOFs, that is, platform surge, heave, pitch motion about P, TMD translation, and tower rotation. On

the left side, M_i^j and I_i^j denote generalized mass and generalized inertial tensor for DOF i with regard to DOF j. On the right side, gr, hdr, moor, ctr, spr, and damp describe gravitational, hydro, centripetal, spring, and damping effects in forces and moments. Expanded expressions of this model for TMD platform installation are presented in the appendix, and the detailed term descriptions are listed in Table 2.

The mass matrix on the left side of (6) exhibits the system inertial property, that is, mass and inertia tensor, and it also includes hydro added mass and acceleration coupling terms. The terms on the right side of (6) are external loads, which can be classified into several different effects. Gravitational forces and moments are the first type of loads, labeled as gr. The second effect, labeled as hdr·moor, is the hydrodynamic and mooring loading, which consists of hydrostatics, vicious drag, radiation damping, additional linear damping, and mooring effects. The third type, which is produced by D'Alembert's principle, is the centripetal forces and moments which originate from the rotation of platform, tower, and TMD about the reference point P, and they are labeled as ctr. Tower and platform interaction is the fourth effect captured in this equation, and the bending moment is described by a linear spring-damper between them. The final consideration is the spring and damping effect in TMD, so it is labeled as spr·damp.

After obtaining the OC3-Hywind dynamic model for its surge-heave-pitch motion in still water, parameter identification and validation should be performed to quantize the unknown parameters and verify the correctness of the proposed model. The parameter estimation is accomplished by minimizing the output difference between FAST-SC and the established model. Based on the estimation result, free decay response comparison for the OC3-Hywind surge-pitch-heave motion without TMD is illustrated in Figure 3, where two results coincide well with each other. Then, in order to further validate the established model, free decay response comparisons are performed again with TMD installed in nacelle. In practice, there exist space limitations for the nacelle, so the TMD displacement should be restricted into a certain range. According to the nacelle dimensions defined in [21], the TMD displacement range is determined as ±7 m in this work. In FAST-SC, the TMD motion constraints were modelled as stops, where there would be spring stiffness and damping interaction between TMD and nacelle or platform when its displacement exceeds the user defined constraints. The stops effect in this work is characterized in the same way. Figure 4 illustrates the free decay response comparison results with TMD stops. As expected, the established model still manages to capture the system dynamics including TMD stop interactions. It is worth mentioning that the stops with various spring and damping coefficients could have quite different impacts on system dynamics, but further analysis of stop parameters is not within the scope of this paper.

Based on the above analysis, the proposed model has captured most of the intrinsic dynamics for OC3-Hywind surge-heave-pitch motion, including hydrodynamic and mooring loads, tower flexibility, and TMD-nacelle interaction. Next step is to tune TMD parameters for effective system load reduction.

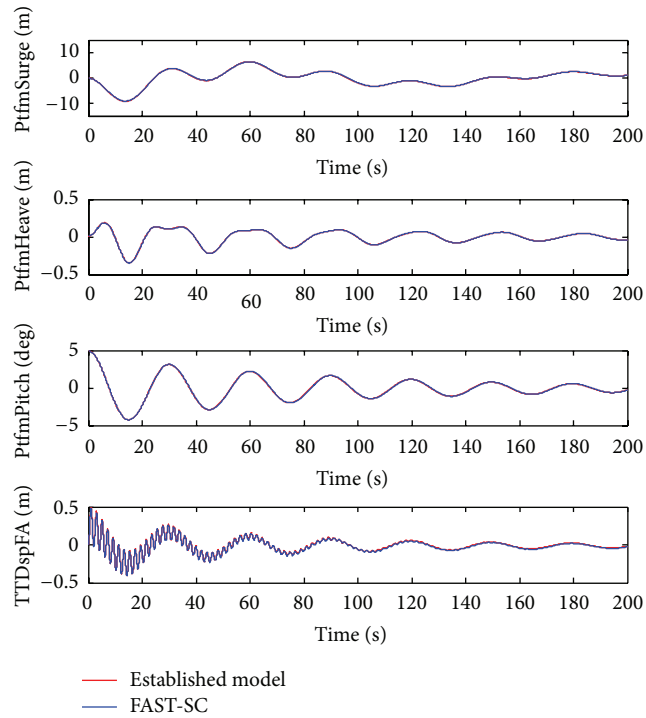

Figure 3: Free decay response comparison between identified model and FAST-SC numerical simulation for surge-pitch-heave motion without TMD (5° initial platform pitch).

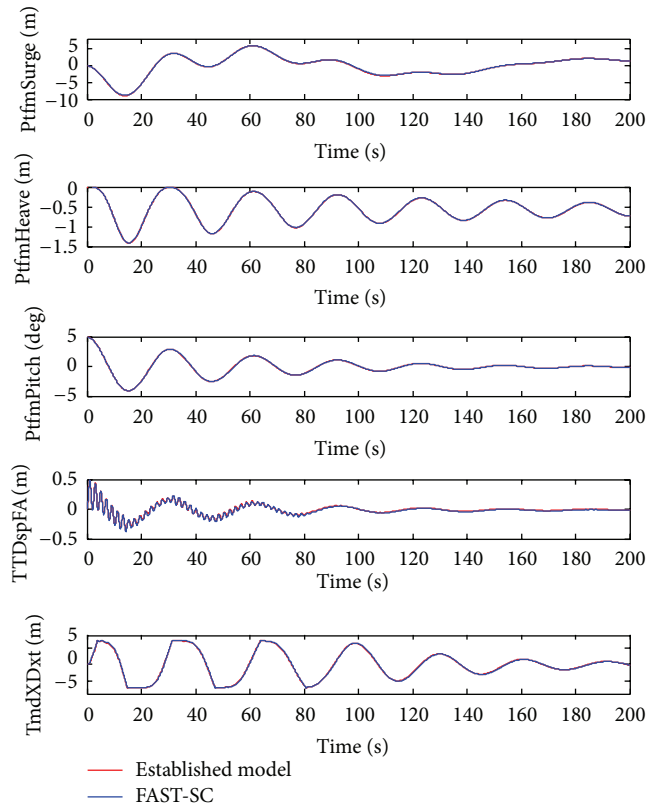

Figure 4: Free decay response comparison with TMD and stops in nacelle.

3. Parameter Tuning

Optimal parameter tuning of the vibration absorber is an important design consideration in passive structural control problems. The design aim in this work is to find the optimal TMD coefficients for wind turbine load reduction. The parameters to be determined include TMD spring and damping coefficients. TMD mass is not parametrically studied in this work since it is usually determined by cost and heavier mass will more likely produce better performance. Specifically, in order to be consistent with [11], the mass is chosen to be 20,000 kg, which takes about 3.33% of the weight for tower-RNA structure.

In fact, the most convincing solution here is to try all possible values of these parameters in FAST-SC. However, this global searching process will take tens of thousands of calls from FAST-SC, and it usually will take minutes to run it for only one time. Therefore, exhaustive search is almost impossible with ordinary computers, and appropriate optimization methods are needed. Based on the established model, in this section, three different methods are used for this parameter tuning problem.

3.1. Frequency and Damping Analysis. In engineering applications, the natural frequency of TMD is usually tuned to be near that of the target system; thus, it will effectively dissipate the undesirable system vibration energy. In order to systematically describe this phenomenon, Den Hartog [22] analyzed the response of undamped main system with TMD subjected to harmonic external forces and derived an explicit expression to determine the optimal TMD natural frequency and damping ratio for vibration inhibition. The optimal solution is given by

$$f_{\text{tmd}} = \frac{f}{1+\mu}, \qquad \xi_{\text{tmd}} = \sqrt{\frac{3\mu}{8(1+\mu)}}, \tag{7}$$

where μ denotes the mass ratio m_{tmd}/m and f and ξ are the natural frequency and damping ratio of target system. f_{tmd} and ξ_{tmd} represent the optimal natural frequency and damping ratio of TMD.

In order to adopt this method, eigenanalysis based on model linearization result is performed first to obtain system natural frequencies and damping ratios for the modes of interest.

The eigenanalysis result has been presented in [23], where natural frequencies of two most critical modes, that is, platform pitch mode and first tower fore-aft bending mode, are 0.4732 Hz and 0.0342 Hz, and their damping ratios are 0.0087 and 0.1418.

However, in this analysis process, the nonlinearity of TMD stops due to space constraints is not considered, which has been shown to have strong influence on TMD load reduction effectiveness according to the following nonlinear FAST-SC simulation results. Therefore, a more thorough method should be proposed to find the best combination of these TMD parameters.

Table 3: Performance indices.

Index	Description
$J_1 = \sqrt{(1/T)\int_0^T (x_{tt} - \bar{x}_{tt})^2 dt}$	Standard deviation of tower top displacement under its equilibrium point
$J_2 = \max(x_{tt}) - \min(x_{tt})$	Range of tower top displacement

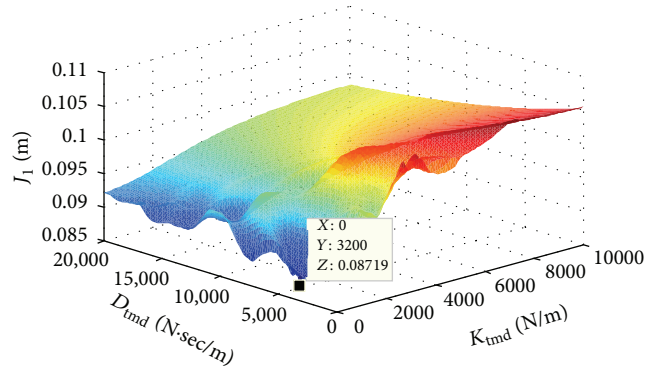

Figure 5: Surface plot subjected to performance index J_1 with TMD installed in nacelle.

3.2. Surface Plot. In the previous section, we have obtained a mathematical model describing OC3-Hywind surge-heave-pitch motion, which manages to capture most of the system structural dynamics, hydro and mooring effects. More importantly, the time for solving this dynamic equation is less than 1s; thus, surface plotting, a global parameter searching method, becomes a possible solution to determine the optimal TMD parameters.

Next, we introduce the performance indices in Table 3 which are used in the optimization process. The tower top fore-aft deflection is the best indicator of tower bottom bending moments, and the author in [14] used standard deviation of tower top displacement as the performance index, which is also adopted in this work as the first performance index J_1. Secondly, we also care about load reduction effectiveness of the proposed method in extreme events; thus, the range of tower top displacement in the free decay test is treated as another evaluation index J_2.

Based on these indices, exhaustive search is performed where TMD spring and damping constants are regarded as two coefficients to be optimized. The parameter range and interval are chosen when both time consumption and accuracy are considered. The surface plots for different design criteria are illustrated in Figures 5 and 6, and the optimization results are listed in Table 4.

Although surface plotting could be regarded as a global optimization method, which produces a relatively comprehensive evaluation of the performance index with possible parameters, it is still computationally expensive, which will take hours or days to finish one optimization process. Also, there might exist better solution if the parameter interval is not small enough. Therefore, more intelligent and efficient optimization algorithms are demanded.

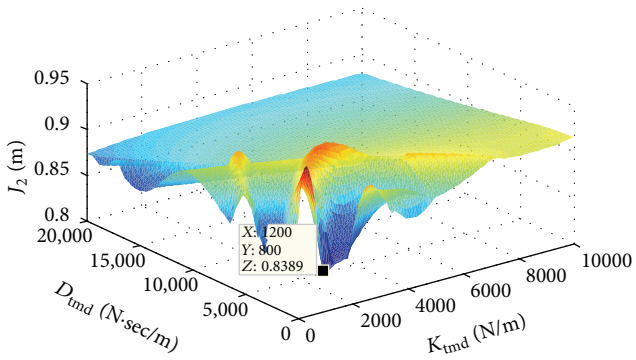

Figure 6: Surface plot subjected to performance index J_2 with TMD installed in nacelle.

Table 4: Parameter optimization result with TMD in nacelle (m_{tmd} = 20,000 kg).

Method	Performance index	K_{tmd} (N/m)	D_{tmd} (N·s/m)
Den Hartog [22]	Tower bending mode (Den1)	165571	12661
Den Hartog [22]	Platform pitch mode (Den2)	865	915
Surface plot	J_1 = 0.0872 m	0	3200
Surface plot	J_2 = 0.8389 m	1200	800
GA	J_1 = 0.0871 m	0	3130
GA	J_2 = 0.7620 m	164231	20889

3.3. Genetic Algorithm. In the past few years, genetic algorithm has been widely applied in a broad spectrum of real-world systems [24–26]. This approach starts with randomly generated population, and individuals with better fitness will be selected as the basis of the next generation. The improved population will keep evolving after inheritance, mutation, selection, and crossover procedures until it meets the final requirement. As a global optimization method, genetic algorithm is based on stochastic variables and does not require the derivatives of object function, which brings the advantages of global evaluation and objective tolerance when compared with other gradient based local optimization methods. It usually helps to obtain a better result in optimization problems with nonsmooth objective functions and thus is suitable for the optimization problem in this work.

When implementing the algorithm, probability of the roulette wheel uniform crossover is chosen as 0.6, and the mutation probability 0.01 is used. Minimum number of generations is set as 20. Optimization results are shown in Table 4. It can be noticed that genetic algorithm gives a better result with respect to J_2 since the surface plotting has a limited searching range.

4. Simulation and Analysis

In this section, based on the optimization result, fully nonlinear simulations are performed in FAST-SC with all wind turbine DOFs enabled. Each test runs for 630 seconds, and the output data in the first 30s are not recorded, waiting for generator torque and blade pitch motion to arrive at normal operation state. The modified generator torque and blade pitch controller from NREL will be used in the form of a dynamic link library for all tests [16].

Table 5: Percentage of load reduction with different TMD tuning results compared with baseline.

Case	Evaluation index	Den1	Den2	J_1	J_2
10 m/s	DEL TwrBsMyt	6.35	0.66	0.52	6.00
	DEL TwrBsMxt	32.18	14.2	11.44	28.37
	DEL RootMyc1	1.07	−0.18	0.10	0.85
	DEL Anch1Ten	0.93	3.01	1.21	0.93
	95th TwrBsMyt	−2.00	−4.04	−3.89	−2.00
	95th TwrBsMxt	6.01	2.7	2.55	5.06
	95th PtfmPitch	−2.08	−1.96	−2.08	−2.08
	95th PtfmRoll	−1.67	0.21	0.13	−1.67
18 m/s	DEL TwrBsMyt	3.61	7.77	8.78	3.35
	DEL TwrBsMxt	25.55	0.98	−3.94	21.24
	DEL RootMyc1	1.07	4.99	5.93	1.14
	DEL Anch1Ten	1.15	0.32	0.32	1.14
	95th TwrBsMyt	−3.15	5.02	6.48	−3.25
	95th TwrBsMxt	7.90	4.70	1.69	7.10
	95th PtfmPitch	−1.05	10.66	12.43	−1.04
	95th PtfmRoll	6.55	15.54	14.32	6.58
	RMS GenPwr	−5.46	21.09	29.22	−5.41
37 m/s	DEL TwrBsMyt	1.47	−19.95	−16.25	1.22
	DEL TwrBsMxt	0.14	0.51	0.42	0.18
	DEL RootMyc1	1.80	−45.71	−28.34	2.03
	DEL Anch1Ten	1.33	1.83	0.96	0.78
	95th TwrBsMyt	−0.78	−4.88	−2.33	−0.77
	95th TwrBsMxt	0.41	0.40	0.25	0.47
	95th PtfmPitch	4.41	5.40	4.44	4.41
	95th PtfmRoll	−0.30	−0.63	−0.57	−0.30

The wind and wave conditions in the experiment are defined almost the same as in [12]. For wind condition, both the above and below rated wind speeds are considered, and mean value of turbulent wind is defined as 18 m/s and 10 m/s separately. The turbulent wind file is generated by TurbSim, where Kaimal spectra and the power law exponent of 0.14 are used according to the IEC61400-3 offshore wind turbine design standard. The normal turbulence intensity is set as 15% (18 m/s case) and 18% (10 m/s case). Random seed in this work is arbitrarily chosen as 231857312. In order to define the wave condition, JONSWAP spectrum is utilized to generate the stochastic wave inputs. The significant wave height is set as 2.3 m (10 m/s case) and 3.7 m (18 m/s case), and the peak spectral period is defined as 14 s. Besides, the parked situation is also considered assuming the turbine suffers extreme 50-year storm, that is, 37 m/s turbulent wind with power law exponent of 0.11 and 11% turbulence intensity. Wave height and period are defined as 13.8 m and 19 s.

Percentage of load reduction with different TMD parameter choice is shown in Table 5. In order to measure the fatigue and extreme loading, damage equivalent load (DEL) and the

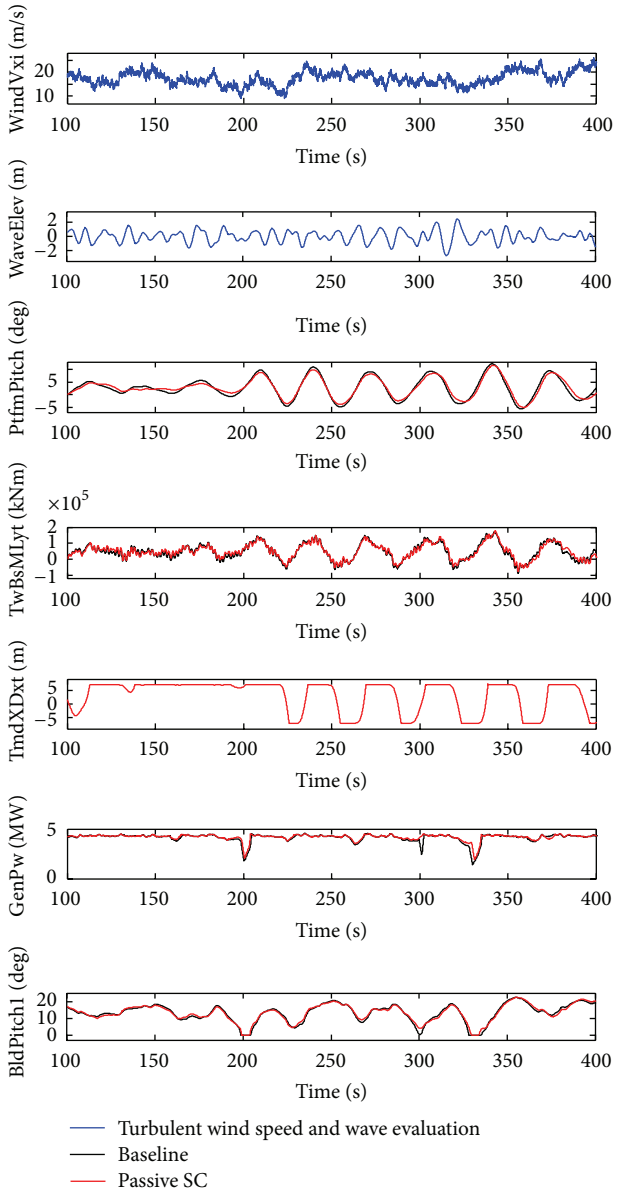

FIGURE 7: FAST-SC simulation results with 18 m/s turbulent wind and 3.7 m significant height wave.

95th percentile of fore-aft and side-side tower base bending moments (TwrBsMyt and TwrBsMxt) and flapwise bending moment at the first blade root (RootMyc1) are calculated, together with the 95th percentile of platform pitch and roll rotation angle. In the above rated situation, the root mean square (RMS) of generated power is considered as another index.

It can be seen from results that the design of TMD with small spring and damping coefficients will achieve much load reduction in the above rated condition, where one simulation result is shown in Figure 7. However, it will deteriorate system performance when the turbine is working in the below rated or parked situations. In contrast, the design with large spring and damping constants will produce moderate load reduction in all working conditions.

5. Conclusion

This work focuses on the modeling and parameter tuning of a passive structural control design for the OC3-Hywind floating wind turbine. Firstly, the coupled surge-heave-pitch dynamic model with a TMD installed in nacelle is established based on the D'Alembert's principle. Parameter estimation is also performed for model validation. Then, different parameter tuning methods and performance indices are used for TMD parameter determination. FAST-SC is used for fully coupled nonlinear simulation with various wind and wave conditions. The results show that the design of TMD with small spring and damping coefficients will achieve much load reduction in the above rated condition, but it will deteriorate system performance when the turbine is working in the below rated or parked situations. In contrast, the design with large spring and damping constants will produce moderate load reduction in all working conditions. Therefore, inappropriate TMD design will not contribute to wind turbine load reduction. Besides, only enabling TMD in certain range of wind speed might be a possible solution for this design. Further real experiments need to be conducted to verify this idea. Future work will also consider the situation when TMD is installed in the spar itself or other types of platforms.

Appendix

Consider the following:

$$M_{\mathrm{sg}}^{\mathrm{sg}} = A_{\mathrm{sg}}^{\mathrm{sg}} + m_{\mathrm{ptfm}} + m_{\mathrm{twr}} + m_{\mathrm{rna}} + m_{\mathrm{tmd}},$$

$$I_{\mathrm{sg}}^{p} = A_{\mathrm{sg}}^{p} + m_{\mathrm{twr}}\left(L_{\mathrm{twr}} + L_{\mathrm{jot}}\right)\cos\theta_p - m_{\mathrm{ptfm}}L_{\mathrm{ptfm}}\cos\theta_p,$$

$$M_{\mathrm{sg}}^{\mathrm{tmd}} = M_{\mathrm{tmd}}^{\mathrm{sg}} = m_{\mathrm{tmd}}\cos\left(\theta_p + \sin\left(\theta_t - \theta_p\right)L_{\mathrm{rna}}\dot{\Phi}_{\mathrm{rna}}\right),$$

$$I_{\mathrm{sg}}^{t} = m_{\mathrm{rna}}\left(L_{\mathrm{rna}} + L_{\mathrm{jot}}\right)\cos\theta_t + m_{\mathrm{tmd}}L_{\mathrm{rna}}\cos\theta_t,$$

$$M_{\mathrm{hv}}^{\mathrm{hv}} = A_{\mathrm{hv}}^{\mathrm{hv}} + m_{\mathrm{ptfm}} + m_{\mathrm{twr}} + m_{\mathrm{rna}} + m_{\mathrm{tmd}},$$

$$I_{\mathrm{hv}}^{p} = -m_{\mathrm{twr}}\left(L_{\mathrm{twr}} + L_{\mathrm{jot}}\right)\sin\theta_p + m_{\mathrm{ptfm}}L_{\mathrm{ptfm}}\sin\theta_p,$$

$$M_{\mathrm{hv}}^{\mathrm{tmd}} = M_{\mathrm{tmd}}^{\mathrm{hv}} = -m_{\mathrm{tmd}}\sin\left(\theta_p + \sin\left(\theta_t - \theta_p\right)L_{\mathrm{rna}}\dot{\Phi}_{\mathrm{rna}}\right),$$

$$I_{\mathrm{hv}}^{t} = -m_{\mathrm{rna}}\left(L_{\mathrm{rna}} + L_{\mathrm{jot}}\right)\sin\theta_t - m_{\mathrm{tmd}}L_{\mathrm{rna}}\sin\theta_t,$$

$$M_{p}^{\mathrm{sg}} = A_{p}^{\mathrm{sg}} + m_{\mathrm{rna}}\left(L_{\mathrm{rna}} + L_{\mathrm{jot}}\right)\cos\theta_t + m_{\mathrm{twr}}\left(L_{\mathrm{twr}} + L_{\mathrm{jot}}\right)\cos\theta_p - m_{\mathrm{ptfm}}L_{\mathrm{ptfm}}\cos\theta_p + m_{\mathrm{tmd}}\left(L_{\mathrm{rna}} + L_{\mathrm{jot}}\right)\cos\theta_t,$$

$$
\begin{aligned}
M_p^{\mathrm{hv}} &= -m_{\mathrm{rna}}\left(L_{\mathrm{rna}}+L_{\mathrm{jot}}\right)\sin\theta_t \\
&\quad -m_{\mathrm{twr}}\left(L_{\mathrm{twr}}+L_{\mathrm{jot}}\right)\sin\theta_p \\
&\quad +m_{\mathrm{ptfm}}L_{\mathrm{ptfm}}\sin\theta_p - m_{\mathrm{tmd}}\left(L_{\mathrm{rna}}+L_{\mathrm{jot}}\right)\sin\theta_t, \\
I_p^p &= A_p^p + J_{\mathrm{ptfm}}^{\mathrm{CG_{ptfm}}} + m_{\mathrm{ptfm}}L_{\mathrm{ptfm}}^2 + J_{\mathrm{twr}}^{\mathrm{CG_{twr}}} \\
&\quad + m_{\mathrm{twr}}\left(L_{\mathrm{twr}}+L_{\mathrm{jot}}\right)^2 + m_{\mathrm{rna}}\left(L_{\mathrm{rna}}+L_{\mathrm{jot}}\right)^2 \\
&\quad + m_{\mathrm{tmd}}\left(L_{\mathrm{rna}}+L_{\mathrm{jot}}\right)^2, \\
I_{\mathrm{tmd}}^p &= 0, \qquad M_{\mathrm{tmd}}^{\mathrm{tmd}} = m_{\mathrm{tmd}}, \\
I_{\mathrm{tmd}}^t &= M_t^{\mathrm{tmd}} = m_{\mathrm{tmd}}L_{\mathrm{rna}}\cos\left(\sin\left(\theta_t-\theta_p\right)L_{\mathrm{rna}}\dot{\Phi}_{\mathrm{rna}}\right), \\
M_t^{\mathrm{sg}} &= m_{\mathrm{rna}}L_{\mathrm{rna}}\cos\theta_t + m_{\mathrm{twr}}L_{\mathrm{twr}}\cos\theta_p \\
&\quad + m_{\mathrm{tmd}}L_{\mathrm{rna}}\cos\theta_t, \\
M_t^{\mathrm{hv}} &= -m_{\mathrm{rna}}L_{\mathrm{rna}}\sin\theta_t - m_{\mathrm{twr}}L_{\mathrm{twr}}\sin\theta_p \\
&\quad - m_{\mathrm{tmd}}L_{\mathrm{rna}}\sin\theta_t, \\
\dot{\Phi}_{\mathrm{rna}} &= \left.\frac{\partial\Phi(h)}{\partial h}\right|_{h=L_{\mathrm{rna}}}, \\
F_{\mathrm{hv}}^{\mathrm{gr}} &= -\left(m_{\mathrm{ptfm}}+m_{\mathrm{twr}}+m_{\mathrm{rna}}+m_{\mathrm{tmd}}\right)g, \\
\tau_p^{\mathrm{gr}} &= m_{\mathrm{rna}}\left(L_{\mathrm{rna}}+L_{\mathrm{jot}}\right)\sin\theta_t \\
&\quad + m_{\mathrm{twr}}g\left(L_{\mathrm{twr}}+L_{\mathrm{jot}}\right)\sin\theta_p \\
&\quad - m_{\mathrm{ptfm}}gL_{\mathrm{ptfm}}\sin\theta_p - m_{\mathrm{rna}}gL_d\cos\theta_t \\
&\quad + m_{\mathrm{tmd}}gx_{\mathrm{tmd}}\cos\theta_t + m_{\mathrm{tmd}}g\left(L_{\mathrm{rna}}+L_{\mathrm{jot}}\right)\sin\theta_t, \\
F_{\mathrm{tmd}}^{\mathrm{gr}} &= m_{\mathrm{tmd}}g\sin\left(\theta_p+\sin\left(\theta_t-\theta_p\right)L_{\mathrm{rna}}\dot{\Phi}_{\mathrm{rna}}\right), \\
\tau_t^{\mathrm{gr}} &= m_{\mathrm{twr}}gL_{\mathrm{twr}}\sin\theta_p + m_{\mathrm{rna}}gL_{\mathrm{rna}}\sin\theta_t \\
&\quad - m_{\mathrm{rna}}gL_d\cos\theta_t \\
&\quad + m_{\mathrm{tmd}}gx_{\mathrm{tmd}}\cos\theta_t + m_{\mathrm{tmd}}gL_{\mathrm{rna}}\sin\theta_t, \\
F_{\mathrm{sg}}^{\mathrm{hdr.moor}} &= -D_{\mathrm{sg}}^{\mathrm{sg}}\dot{x}_{\mathrm{sg}} - \widehat{D}_{\mathrm{sg}}^{\mathrm{sg}}\dot{x}_{\mathrm{sg}}^2 - K_{\mathrm{sg}}^{\mathrm{sg}}x_{\mathrm{sg}} - D_{\mathrm{sg}}^p\dot{\theta}_p - K_{\mathrm{sg}}^p\theta_p, \\
F_{\mathrm{hv}}^{\mathrm{hdr.moor}} &= -D_{\mathrm{hv}}^{\mathrm{hv}}\dot{x}_{\mathrm{hv}} - K_{\mathrm{hv}}^{\mathrm{hv}}x_{\mathrm{hv}} - F_{\mathrm{moor}} + F_{\mathrm{buoy}} \\
&\quad - K_{\mathrm{hv}}^{p.\mathrm{sg}}\left(x_{\mathrm{sg}} - L_{\mathrm{moor}}\sin\theta_p\right)^2, \\
\tau_p^{\mathrm{hdr.moor}} &= -D_p^p\dot{\theta}_p - K_p^p\theta_p - D_{\mathrm{p}}^{\mathrm{sg}}\dot{x}_{\mathrm{sg}} - \widehat{D}_p^{\mathrm{sg}}\dot{x}_{\mathrm{sg}}^2 - K_p^{\mathrm{sg}}x_{\mathrm{sg}}, \\
F_{\mathrm{sg}}^{\mathrm{ctr}} &= m_{\mathrm{twr}}\dot{\theta}_p^2\left(L_{\mathrm{twr}}+L_{\mathrm{jot}}\right)\sin\theta_p \\
&\quad + m_{\mathrm{rna}}\dot{\theta}_t^2\left(L_{\mathrm{rna}}+L_{\mathrm{jot}}\right)\sin\theta_t \\
&\quad - m_{\mathrm{ptfm}}\dot{\theta}_p^2L_{\mathrm{ptfm}}\sin\theta_p \\
&\quad + m_{\mathrm{tmd}}\dot{\theta}_t\left(\dot{\theta}_t\left(L_{\mathrm{rna}}+L_{\mathrm{jot}}\right)-\dot{x}_{\mathrm{tmd}}\right)\sin\theta_t, \\
F_{\mathrm{hv}}^{\mathrm{ctr}} &= m_{\mathrm{twr}}\dot{\theta}_p^2\left(L_{\mathrm{twr}}+L_{\mathrm{jot}}\right)\cos\theta_p \\
&\quad + m_{\mathrm{rna}}\dot{\theta}_t^2\left(L_{\mathrm{rna}}+L_{\mathrm{jot}}\right)\cos\theta_t \\
&\quad - m_{\mathrm{ptfm}}\dot{\theta}_p^2L_{\mathrm{ptfm}}\cos\theta_p \\
&\quad + m_{\mathrm{tmd}}\dot{\theta}_t\left(\dot{\theta}_t\left(L_{\mathrm{rna}}+L_{\mathrm{jot}}\right)-\dot{x}_{\mathrm{tmd}}\right)\cos\theta_t, \\
\tau_p^{\mathrm{ctr}} &= \tau_t^{\mathrm{ctr}} = -m_{\mathrm{tmd}}\dot{\theta}_t\left(\dot{\theta}_t\left(L_{\mathrm{rna}}+L_{\mathrm{jot}}\right)-\dot{x}_{\mathrm{tmd}}\right)x_{\mathrm{tmd}}, \\
F_{\mathrm{tmd}}^{\mathrm{spr.damp}} &= -D_{\mathrm{tmd}}\dot{x}_{\mathrm{tmd}} - K_{\mathrm{tmd}}x_{\mathrm{tmd}}, \\
\tau_t^p &= D_t\left(\dot{\theta}_t-\dot{\theta}_p\right) + K_t\left(\theta_t-\theta_p\right).
\end{aligned}
\tag{A.1}
$$

Acknowledgments

This work has been (partially) funded by the Norwegian Centre for Offshore Wind Energy (NORCOWE) under Grant 193821/S60 from the Research Council of Norway (RCN). NORCOWE is a consortium with partners from industry and science, hosted by Christian Michelsen Research. The authors would like to give sincere thanks to Dr. Lackner in University of Massachusetts Amherst for his generosity on the FAST-SC code sharing and Dr. Jonkman from National Renewable Energy Laboratory for his enthusiastic help and support with the specifications of OC3-Hywind model.

References

[1] J. Jonkman, *Dynamics modeling and loads analysis of an offshore floating wind turbine [Ph.D. thesis]*, Department of Aerospace Engineering Sciences, University of Colorado, Boulder, Colo, USA, 2007.

[2] J. M. Jonkman, "Dynamics of offshore floating wind turbines-model development and verification," *Wind Energy*, vol. 12, no. 5, pp. 459–492, 2009.

[3] S. Butterfield, W. Musial, J. Jonkman, P. Sclavounos, and L. Wayman, "Engineering challenges for floating offshore wind turbines," in *Proceedings of the Copenhagen Offshore Wind 2005 Conference and Expedition*, Copenhagen, Denmark, October 2005.

[4] J. Jonkman and D. Matha, "A quantitative comparison of the responses of three floating platform concepts," in *Proceedings of the European Offshore Wind 2009 Conference and Exhibition*, pp. 14–16, 2009.

[5] T. J. Larsen and T. D. Hanson, "A method to avoid negative damped low frequent tower vibrations for a floating, pitch controlled wind turbine," *Journal of Physics*, vol. 75, no. 1, Article ID 012073, 2007.

[6] S. Korkmaz, "A review of active structural control: challenges for engineering informatics," *Computers and Structures*, vol. 89, no. 23-24, pp. 2113–2132, 2011.

[7] P. J. Murtagh, A. Ghosh, B. Basu, and B. M. Broderick, "Passive control of wind turbine vibrations including blade/tower interaction and rotationally sampled turbulence," *Wind Energy*, vol. 11, no. 4, pp. 305–317, 2008.

[8] S. Colwell and B. Basu, "Tuned liquid column dampers in offshore wind turbines for structural control," *Engineering Structures*, vol. 31, no. 2, pp. 358–368, 2009.

[9] J. Li, Z. Zhang, and J. Chen, "Experimental study on vibration control of offshore wind turbines using a ball vibration absorber," *Energy and Power Engineering*, vol. 4, no. 3, pp. 153–157, 2012.

[10] J. Jonkman and M. Buhl Jr., "Fast users guide," Tech. Rep. NREL/EL-500-29798, National Renewable Energy Laboratory, Golden, Colo, USA, 2005.

[11] M. A. Lackner and M. A. Rotea, "Passive structural control of offshore wind turbines," *Wind Energy*, vol. 14, no. 3, pp. 373–388, 2011.

[12] M. A. Lackner and M. A. Rotea, "Structural control of floating wind turbines," *Mechatronics*, vol. 21, no. 4, pp. 704–719, 2011.

[13] G. M. Stewart and M. A. Lackner, "The effect of actuator dynamics on active structural control of offshore wind turbines," *Engineering Structures*, vol. 33, no. 5, pp. 1807–1816, 2011.

[14] G. Stewart, *Load reduction of floating wind turbines using tuned mass dampers [M.S. thesis]*, University of Massachusetts Amherst, Amherst, Mass, USA, 2012.

[15] G. M. Stewart and M. A. Lackner, "Offshore wind turbine load reduction employing optimal passive tuned mass damping systems," *IEEE Transactions on Control Systems Technology*, vol. 21, no. 4, pp. 1090–1104, 2013.

[16] J. Jonkman, "Definition of the floating system for phase iv of oc3," Tech. Rep. NREL/TP- 500-38060, National Renewable Energy Laboratory, Golden, Colo, USA, 2009.

[17] H. Namik and K. Stol, "Performance analysis of individual blade pitch control of offshore wind turbines on two floating platforms," *Mechatronics*, vol. 21, no. 4, pp. 691–703, 2011.

[18] J. Jonkman, S. Butterfield, W. Musial, and G. Scott, "Definition of a 5-mw reference wind turbine for offshore system development," Tech. Rep. NREL/TP-500-47535, National Renewable Energy Laboratory, Golden, Colo, USA, 2009.

[19] S. Rao and R. Durgaiah, *Engineering Mechanics*, Universities Press, Andhra Pradesh, India, 2005.

[20] J. Newman, *Marine Hydrodynamics*, MIT press, Cambridge, Mass, USA, 1977.

[21] H. Kooijman, C. Lindenbug, D. Winkelaar, and E. Van der Hooft, "Dowec 6 mw predesign: aeroelastic modeling of the dowec 6 mw pre-design in phatas," Tech. Rep. DOWEC-F1W2-HJK-01-046/9, Energy research Centre of the Netherlands, Amsterdam, The Netherlands, 2003.

[22] J. P. Den Hartog, *Mechanical Vibrations*, Dover, New York, NY, USA, 1985.

[23] D. Matha, "Model development and loads analysis of an offshore wind turbine on a tension leg platform with a comparison to other floating turbine concepts," Tech. Rep. NREL/SR-500-45891, National Renewable Energy Laboratory (NREL), Golden, Colo, USA, 2010.

[24] H. Wang and H. Ohmori, "Elasto-plastic analysis based truss optimization using genetic algorithm," *Engineering Structures*, vol. 50, pp. 1–12, 2013.

[25] J. D. Poirier, S. S. Vel, and V. Caccese, "Multi-objective optimization of laser-welded steel sandwich panels for static loads using a genetic algorithm," *Engineering Structures*, vol. 49, pp. 508–524, 2013.

[26] F. B. Ramires, S. A. L. d. Andrade, P. C. G. d. S. Vellasco, and L. R. O. d. Lima, "Genetic algorithm optimization of composite and steel endplate semi-rigid joints," *Engineering Structures*, vol. 45, pp. 177–191, 2012.